Johann Radon Institute for
Computational and Applied Mathematics
Austrian Academy of Sciences (ÖAW)

Variational-monolithic ALE fluid-structure interaction: Comparison of computational cost and mesh regularity using different mesh motion techniques

T. Wick

RICAM-Report 2016-12

Variational-monolithic ALE fluid-structure interaction: Comparison of computational cost and mesh regularity using different mesh motion techniques

Thomas Wick

Abstract In this contribution, different mesh motion models for fluid-structure interaction (FSI) are revisited. The FSI problem is formulated by variational-monolithic coupling in the reference configuration employing the arbitrary-Lagrangian Eulerian (ALE) framework. The goal is to further analyze three different mesh motion models; namely nonlinear harmonic, nonlinear elastic, and linear biharmonic. The novelty in this contribution is a detailed computational analysis of the regularity of the ALE mapping and cost complexity for the nonstationary FSI-2 benchmark problem with large solid deformations.

1 Introduction

The purpose of this study is on further comparisons of mesh motion models for arbitrary-Lagrangian Eulerian (ALE) fluid-structure interaction (FSI) problems. The extension to existing studies for variational-monolithic ALE-FSI is a computational analysis of the regularity of the ALE mapping, the number of Newton iterations, and computational complexity of matrix assemblings and linear solves.

To realize the geometric coupling that is necessary to move the fluid mesh, a common methodology is to solve an auxiliary PDE, the so-called mesh motion PDE (MMPDE) [15, 14, 3, 21, 11, 4, 2, 5, 10, 1]. Comparisons of different MMPDEs have been performed in [7, 22, 17]. In this study, we refine our previous 2nd order models [17] and use nonlinear harmonic and nonlinear elastic models and compare them with the (linear) biharmonic MMPDE. Of course, the biharmonic equation is

Thomas Wick
Fakultät für Mathematik, Lehrstuhl M17, Technische Universität München, Boltzmannstr. 3, 85747 Garching near München, Germany, e-mail: wick@ma.tum.de
and
RICAM, Austrian Academy of Sciences, Altenberger Str. 69, 4040 Linz, Austria, e-mail: thomas.wick@ricam.oeaw.ac.at

much more expensive to solve since either C^1 continuous finite elements are required or Ciarlet's splitting into a first order system. However, in [17], it was never systematically analyzed that the 4th order biharmonic equation is linear but the 2nd order models are, firstly, nonlinear, and secondly, have worse regular ALE mappings. Consequently, it is a priori not clear if the biharmonic MMPDE is really (always) inferior in terms of computational cost because the linear solve is indeed more expensive but it might have less Newton steps per time step due to a better ALE regularity. To answer this key question, the present study addresses:

- Computational analysis of the regularity of the ALE mapping (observing $min(\hat{J})$);
- Observation of the number of Newton steps at each time step for (very) large deformations for a long-term FSI computation;
- Relation of the ALE-regularity and number of Newton steps with conclusions on the total computational cost for a serial programming code.

These goals will be investigated for the challenging FSI benchmark test FSI-2 [10]. Here, systematic studies for all three MMPDEs with different time step sizes and on different spatial mesh levels are carried out. Of course, for other configurations, in particular for smaller solid deformations, the results might differ significantly. Thus, it still holds the golden rule: the application determines the method! A related study for quasi-stationary FSI (with moderate flow) investigating the differentiability (theory and simulations) of the FSI solution map for large solid deformations has been carried out in [20].

The outline of this paper is as follows: In Section 2, we recapitulate fluid-structure interaction with variational-monolithic coupling formulated in the reference domain. Additionally, three mesh motion models are recapitulated. Next, in Section 3, the discretization and solution algorithm are briefly recalled. In the final Section 4, a nonstationary FSI problem (Hron/Turek's FSI 2 benchmark [10]) with large solid deformations is computed. As programming code, the open-source FSI-code published in [18] has been employed for the fourth-order biharmonic mesh motion technique. This code has been modified for working with second order models.

2 The coupled FSI problem in the reference domain

2.1 Notation and spaces

We denote by $\Omega := \Omega(t) \subset \mathbb{R}^d$, $d = 2$, the domain of the fluid-structure interaction problem. This domain consists of two time-dependent subdomains $\Omega_f(t)$ and $\Omega_s(t)$. The interface between both domain is denoted by $\Gamma_i(t) = \partial\Omega_f(t) \cap \partial\Omega_s(t)$. The initial (or later reference) domains are denoted by $\widehat{\Omega}_f$ and $\widehat{\Omega}_s$, respectively, with the interface $\widehat{\Gamma}_i = \partial\widehat{\Omega}_f \cap \partial\widehat{\Omega}_s$. Furthermore, we denote the outer boundary by $\partial\widehat{\Omega} = \widehat{\Gamma} = \widehat{\Gamma}_D \cup \widehat{\Gamma}_N$ where $\widehat{\Gamma}_D$ and $\widehat{\Gamma}_N$ denote Dirichlet and Neumann boundaries, re-

spectively. For the convenience of the reader and when we expect no confusion, we omit the explicit time-dependence and we use $\Omega := \Omega(t)$ to indicate time-dependent domains. Throughout this paper, we indicate with 'f' and 's' indices, fluid and structure related terms, respectively. We often use the standard notion for L^2 scalar products defined in a function space X:

$$(a,b) = \int_\Omega a \cdot b\, dx, \quad \text{for } a,b \in X^d, \quad (A,B) = \int_\Omega A : B\, dx, \quad \text{for } A,B \in X^{d\times d},$$

where d denotes the dimension of the problem (in this paper $d = 2$). We expect that the reader is familiar with vector-valued PDEs and do not mention any more explicitly the dimension d. For the function spaces, we set:

$$\begin{aligned}
\hat{L}_f &:= L^2(\widehat{\Omega}_f), \quad \hat{L}_s := L^2(\widehat{\Omega}_s), \quad \hat{L}^0_f := L^2(\widehat{\Omega}_f)/\mathbb{R},\\
\hat{L}^0_s &:= L^2(\widehat{\Omega}_s)/\mathbb{R}, \quad \hat{V}^0_f := \hat{V}^0_{\widehat{\Omega}_f}, \quad \hat{V}^0_s := \hat{V}^0_{\widehat{\Omega}_s},\\
\hat{V}^0_{f,\hat{v}} &:= \{\hat{v}_f \in H^1_0(\widehat{\Omega}_f) : \hat{v}_f = \hat{v}_s \text{ on } \widehat{\Gamma}_i\},\\
\hat{V}^0_{f,\hat{u}} &:= \{\hat{u}_f \in H^1_0(\widehat{\Omega}_f) : \hat{u}_f = \hat{u}_s \text{ on } \widehat{\Gamma}_i\},\\
\hat{V}^0_{f,\hat{u},\widehat{\Gamma}_i} &:= \{\hat{\psi}_f \in H^1_0(\widehat{\Omega}_f) : \hat{\psi}_f = \hat{\psi}_s \text{ on } \widehat{\Gamma}_i \subset \partial X\}.
\end{aligned}$$

2.2 The ALE mapping

Firstly, we define the ALE transformation:

Definition 1 *The ALE mapping is defined in terms of the vector-valued fluid mesh displacement $\hat{u}_f : \widehat{\Omega}_f \to \mathbb{R}^d$ such that*

$$\hat{\mathscr{A}}(\hat{x},t) : \widehat{\Omega}_f \times I \to \Omega_f, \quad \textit{with } \hat{\mathscr{A}}(\hat{x},t) = \hat{x} + \hat{u}_f(\hat{x},t), \tag{1}$$

which is specified through the deformation gradient and its determinant

$$\widehat{F} := \widehat{\nabla}\hat{\mathscr{A}} = \hat{I} + \widehat{\nabla}\hat{u}_f, \quad \hat{J} := det(\widehat{F}). \tag{2}$$

Furthermore, function values in Eulerian and Lagrangian coordinates are identified by

$$u_f(x) =: \hat{u}_f(\hat{x}), \quad \textit{with } x = \hat{\mathscr{A}}(\hat{x},t). \tag{3}$$

The mesh velocity is defined by $w := \partial_t \hat{\mathscr{A}}$. The mesh velocity is numerically realized as $w = \partial\hat{\mathscr{A}} = \frac{\hat{u}_f - \hat{u}^{n-1}_f}{k}$, where $\hat{u}_f$ is the current displacement solution and $\hat{u}^{n-1}_f$ the previous time step solution, and $k := t^n - t^{n-1}$ being the time step size. The key quantity to measure the regularity of the fluid mesh is $\hat{J}$.

To formulate FSI in ALE coordinates, there are two possible ways presented in the literature:

- ALE$_{dm}$ (explicit mesh moving): the fluid equations are computed on the deformed configuration Ω and the mesh is moved explicitely.
- ALE$_{fx}$ (implicit mesh moving): all fluid equations are transformed onto the fixed reference configuration $\widehat{\Omega}$ and the mesh movement is 'hidden' in the transformations $\widehat{F}$ and $\hat{J}$.

In our work, we employ this second possibility; namely ALE$_{fx}$.

2.3 Interface coupling conditions on $\widehat{\Gamma_i}$

The coupling of a fluid with solid equations must satisfy three conditions as displayed in Figure 1:

- continuity of velocities;
- continuity of normal stresses;
- continuity of displacements (coupling of physical solids and fluid mesh motion).

The first two conditions are of physical nature whereas the latter one has geometrical meaning. Mathematically, the first and third condition can be classified as (non-homogeneous) Dirichlet conditions and the second condition is a (non-homogeneous) Neumann condition.

In variational-monolithic coupling these Dirichlet conditions are built into the corresponding Sobolev spaces. Neumann type conditions are weakly incorporated through interface integrals (but actually disappear in the later models because of their weak continuity).

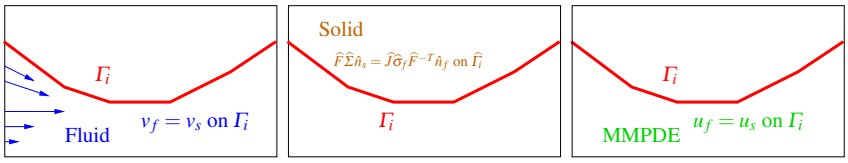

Fig. 1 Illustration of the three coupling conditions on Γ_i (respectively its corresponding definition on the fixed $\widehat{\Gamma_i}$): v_f is required to solve the fluid system, $\widehat{F}\widehat{\Sigma}_s\hat{n}_s$ is required for the solid system, and u_f is necessary for solving the MMPDE (fluid mesh motion).

2.4 Mesh motion models

The ALE mapping must be a C^1 diffeomorphism in order to have sufficient regularity and invertibility. In function spaces for Galerkin finite elements this condition is expressed through [6]

$$\mathscr{A}_{\hat{}} \in W^{1,\infty}(\widehat{\Omega}) \quad \text{and } \mathscr{A}_{\hat{}}^{-1} \in W^{1,\infty}(\Omega),$$

provided that the boundary is sufficiently smooth. The regularity of $\widehat{\mathscr{A}}$ depends on the mesh motion technique. As three models in this study, we consult two nonlinear second-order models and a linear biharmonic equation:

$$-\widehat{\mathrm{div}}(\widehat{\sigma}_{\mathrm{mesh}}) = 0 \quad \text{in } \widehat{\Omega}_f, \quad \hat{u}_f = \hat{u}_s \text{ on } \widehat{\Gamma}_i, \quad \hat{u}_f = 0 \text{ on } \partial\widehat{\Omega}_f, \tag{4}$$

with

$$\widehat{\sigma}_{\mathrm{mesh}}^{harmonic} = \frac{\alpha_u}{\hat{J}}\widehat{\nabla}\hat{u}_f, \qquad \widehat{\sigma}_{\mathrm{mesh}}^{elastic} = \alpha_\lambda(\mathrm{tr}\widehat{E}_{lin})\hat{I} + 2\alpha_\mu\widehat{E}_{lin},$$

and

$$\alpha_\mu = \frac{\alpha_u}{2\hat{J}(1+\nu_s)},\ \alpha_\lambda = \frac{\nu_s\alpha_u}{\hat{J}(1+\nu_s)(1-2\nu_s)}, \quad \nu_s = -0.1,\ \widehat{E}_{lin} = \frac{1}{2}(\widehat{\nabla}\hat{u}_f + \widehat{\nabla}\hat{u}_f^T).$$

Thirdly, the linear 4th-order biharmonic model reads:

$$\alpha_u\widehat{\Delta}^2\hat{u}_f = 0 \quad \text{in } \widehat{\Omega}_f, \quad \hat{u}_f = \hat{u}_s \text{ and } \partial\hat{u}_f = \partial\hat{u}_s \text{ on } \widehat{\Gamma}_i, \quad \hat{u}_f = \partial\hat{u}_f = 0 \text{ on } \partial\widehat{\Omega}_f.$$

The (small) constant $\alpha_u > 0$ is independent of $\hat{u}_f$.

As previously mentioned in Definition 1, as quantity to measure the ALE regularity, we consult $\hat{J}$. In particular, $\hat{J} > 0$ if $\|\hat{u}_f\|_{W^{2,p}(\widehat{\Omega}_f;\mathbb{R}^d)}$ is sufficiently small, which implies $\widehat{\mathscr{A}}$ and $\widehat{\mathscr{A}}^{-1} \in W^{1,\infty}(\widehat{\Omega};\mathbb{R}^{d\times d})$. Furthermore, the more we bound $\hat{J}$ away from zero, the better the regularity (and hopefully better Newton convergence). In other words, all mesh motion models aim to control $\hat{J}$ and try to bound this quantity away from zero. Here, it is clear from the theoretical standpoint that biharmonic mesh motion leads to higher regularity than second-order harmonic or linear-elastic models. Computational evidence is one purpose of this paper and shown in Section 4.

2.5 A variational-monolithic FSI-formulation using ALE_{fx}

Collecting all pieces for variational-monolithic FSI in ALE_{fx}, we need:

- Fluid momentum and mass conservation: the weak form of isothermal, incompressible Navier-Stokes in ALE_{fx};
- Second-order in time solid momentum in Lagrangian coordinates in mixed form;
- Fluid mesh motion: the weak form $(\widehat{\sigma}_{\mathrm{mesh}}, \widehat{\nabla}\hat{\psi}^u)_{\widehat{\Omega}_f}$ of one of the second-order MMPDEs or alternatively the biharmonic MMPDE.

Then, the weak form of the variational-monolithic FSI model reads:

Formulation 1 (ALE$_{fx}$ FSI with harmonic and elastic mesh motion) *Find vector-valued velocities, vector-valued displacements and a scalar-valued fluid pressure, i.e.,* $\{\hat{v}_f, \hat{v}_s, \hat{u}_f, \hat{u}_s, \hat{p}_f\} \in \{\hat{v}_f^D + \hat{V}_{f,\hat{v}}^0\} \times \hat{L}_s \times \{\hat{u}_f^D + \hat{V}_{f,\hat{u}}^0\} \times \{\hat{u}_s^D + \hat{V}_s^0\} \times \hat{L}_f^0$*, such that* $\hat{v}_f(0) = \hat{v}_f^0$*,* $\hat{v}_s(0) = \hat{v}_s^0$*,* $\hat{u}_f(0) = \hat{u}_f^0$*, and* $\hat{u}_s(0) = \hat{u}_s^0$ *are satisfied, and for almost all times* $t \in (0,T]$ *holds:*

$$
\begin{aligned}
&\textit{Fluid momentum} \begin{cases} (\hat{J}\hat{\rho}_f \partial_t \hat{v}_f, \hat{\psi}^v)_{\widehat{\Omega}_f} + (\hat{\rho}_f \hat{J}(\widehat{F}^{-1}(\hat{v}_f - \hat{w}) \cdot \widehat{\nabla})\hat{v}_f), \hat{\psi}^v)_{\widehat{\Omega}_f} \\ +(\hat{J}\widehat{\sigma}_f \widehat{F}^{-T}, \widehat{\nabla}\hat{\psi}^v)_{\widehat{\Omega}_f} \\ +\langle \rho_f \nu_f \hat{J}(\widehat{F}^T \widehat{\nabla}\hat{v}_f \hat{n}_f)\widehat{F}^{-T}, \hat{\psi}^v \rangle_{\widehat{\Gamma}_{out}} = 0 \quad \forall \hat{\psi}^v \in \hat{V}_{f,\widehat{\Gamma}_i}^0, \end{cases} \\
&\textit{Solid momentum, 1st eq.} \left\{ (\hat{\rho}_s \partial_t \hat{v}_s, \hat{\psi}^v)_{\widehat{\Omega}_s} + (\widehat{F}\widehat{\Sigma}, \widehat{\nabla}\hat{\psi}^v)_{\widehat{\Omega}_s} \quad = 0 \quad \forall \hat{\psi}^v \in \hat{V}_s^0, \right. \\
&\textit{Fluid mesh motion} \left\{ (\widehat{\sigma}_{mesh}, \widehat{\nabla}\hat{\psi}^u)_{\widehat{\Omega}_f} \quad = 0 \quad \forall \hat{\psi}^u \in \hat{V}_{f,\hat{u},\widehat{\Gamma}_i}^0, \right. \\
&\textit{Solid momentum, 2nd eq.} \left\{ \hat{\rho}_s (\partial_t \hat{u}_s - \hat{v}_s, \hat{\psi}^u)_{\widehat{\Omega}_s} \quad = 0 \quad \forall \hat{\psi}^u \in \hat{L}_s, \right. \\
&\textit{Fluid mass conservation} \left\{ (\widehat{div}(\hat{J}\widehat{F}^{-1}\hat{v}_f), \hat{\psi}^p)_{\widehat{\Omega}_f} \quad = 0 \quad \forall \hat{\psi}^p \in \hat{L}_f^0. \right.
\end{aligned}
$$

The stress tensors for fluid and solid read:

$$
\begin{aligned}
\widehat{\sigma}_f &= -\hat{p}_f \hat{I} + 2\hat{\rho}_f \nu_f (\widehat{\nabla}\hat{v}_f \widehat{F}^{-1} + \widehat{F}^{-T}\widehat{\nabla}\hat{v}_f^T), \\
\widehat{\Sigma} &= 2\mu \widehat{E} + \lambda tr\widehat{E}\hat{I}, \quad \widehat{E} = \frac{1}{2}(\widehat{F}^T\widehat{F} - \hat{I}),
\end{aligned}
$$

with the densities $\hat{\rho}_f$ *and* $\hat{\rho}_s$*, fluid's viscosity* ν_f*, the deformation gradient* $\widehat{F}$*, its determinant* $\hat{J}$ *and the identity matrix* $\hat{I}$*. Furthermore, the solid parameters are given by the Lamé parameters* μ_s*,* λ_s*.*

Next, we provide the idea of a monolithic setting for fluid-structure interaction with a biharmonic mesh motion model. To do so, we first formulate the weak form of the biharmonic system as a mixed system in order to apply (later) C^0 finite elements:

Formulation 2 (Weak form of the mixed biharmonic system) *Find a vector-valued* $\hat{\eta}_f \in H^1(\widehat{\Omega})$ *and a vector-valued* $\hat{u}_f \in H_0^1(\widehat{\Omega})$ *such that*

$$
\begin{aligned}
(\hat{\eta}_f, \hat{\psi}^\eta) - (\widehat{\nabla}\hat{u}_f, \widehat{\nabla}\hat{\psi}^\eta) = 0 \quad \forall \hat{\psi}^\eta \in H^1(\widehat{\Omega}), \\
(\widehat{\nabla}\hat{\eta}_f, \widehat{\nabla}\hat{\psi}^u) = 0 \quad \forall \hat{\psi}^u \in H_0^1(\widehat{\Omega}).
\end{aligned}
$$

With these preparations $\widehat{\sigma}_{mesh}$ can be formulated in terms of two equations. The resulting formulation with all details can be found in [19].

3 Discretization and solution algorithm

The fully-coupled problem is solved with the Rothe method: first time, then space. Time discretization is based on second order finite difference schemes as presented

for these settings in [17]. Computational stability of these schemes for long-time computations has been investigated in [16, 13]. In the latter article we have found that smaller time steps are demanded by the solid part of the FSI problem. For numerical stability and no time step restrictions, it is of importance to employ A-stable implicit time-stepping schemes. This is one reason why a monolithic FSI formulation has been adopted. In space, the problem is discretized with conforming finite elements on a quadrilateral mesh. For the fluid, the inf-sup stable parametric Q_2^c/P_1^{dc} velocity-pressure pair is chosen. All displacements are discretized with the Q_2^c element. In the case of the biharmonic MMPDE, the additional displacements are also discretized with Q_2^c elements. The fully-coupled nonlinear problems are treated with Newton's method as explained in detail in [17, 16]. As linear solver we use the direct solver UMFPACK.

4 Numerical test: the FSI-2 benchmark [10]

Configuration

The computational domain has length $L = 2.5m$ and height $H = 0.41m$. The circle center is positioned at $C = (0.2m, 0.2m)$ with radius $r = 0.05m$. The elastic beam has length $l = 0.35m$ and height $h = 0.02m$. The right lower end is positioned at $(0.6m, 0.19m)$, and the left end is attached to the circle.

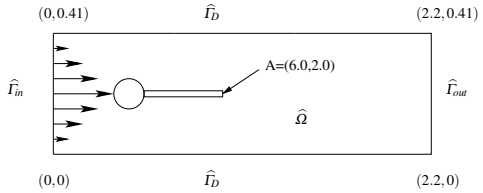

Fig. 2 Flow around cylinder with elastic beam with circle-center $C = (0.2, 0.2)$ and radius $r = 0.05$.

Boundary conditions

For the upper, lower, and left boundaries, the 'no-slip' conditions for velocity and no zero displacement for structure are given. At the outlet $\hat{\Gamma}_{out}$, the 'do-nothing' outflow condition [9] is imposed leading to a zero mean value, i.e., $\int_{\hat{\Gamma}_{out}} p\,ds$ of the pressure at this part of the boundary. A parabolic inflow velocity profile is given on $\hat{\Gamma}_{in}$ by

$$v_f(0,y) = 1.5\bar{U}\frac{4y(H-y)}{H^2}, \quad \bar{U} = 1.0ms^{-1}.$$

Initial conditions

For the non-steady tests one should start with a smooth increase of the velocity profile in time. We use

$$v_f(t;0,y) = \begin{cases} v_f(0,y)\frac{1-\cos(\frac{\pi}{2}t)}{2} & \text{if } t < 2.0s \\ v_f(0,y) & \text{otherwise.} \end{cases}$$

The term $v_f(0,y)$ is already explained above.

Quantities of comparison and their evaluation
The goal functionals are:

1) The y-deflection of the beam at $A(t)$, drag and lift [10].
2) The minimal $\hat{J}$.
3) Number of Newton iterations for lowest and largest deformations.
4) Total computational cost, total matrix assemblings and total linear solves.

Model and material parameters
For the fluid we use $\rho_f = 10^3 kgm^{-3}$, $\nu_f = 10^{-3} m^2 s^{-1}$. The elastic structure is characterized by $\rho_s = 10^4 kgm^{-3}$, $\nu_s = 0.4$, $\mu_s = 5 * 10^5 kgm^{-1}s^{-2}$. The Reynold's number is

$$Re = \frac{L\bar{V}}{\nu} = \frac{0.1 \times 1}{10^{-3}} = 100,$$

where we choose the diameter of the cylinder as characteristic length, $D = 2r = 0.1m$. As characteristic velocity, we take the mean velocity, $\bar{V} = \frac{2}{3}V(0,H/2,t)$ where V is just the parabolic inflow profile from above and evaluated in the middle $H/2$ with the highest velocity:

$$V = v_f(0,H/2) = 1.5 \times 1.0 \frac{4y(H-H/2)}{H^2} = 1.5 \quad \Rightarrow \quad \bar{V} = 1.5 \times V = \frac{2}{3}1.5 = 1.$$

The (absolute) Newton tolerance is chosen as 10^{-8}. The shifted Crank-Nicolson scheme [12, 8] is used for time integration. In one example however the classical Crank-Nicolson scheme has been applied for comparisons. The Jacobian matrix (left hand side of Newton's method) is only build if the ratio between the new Newton residual and the previous one, is larger than 0.1; in the other case we work with quasi-Newton steps using the last Jacobian matrix.

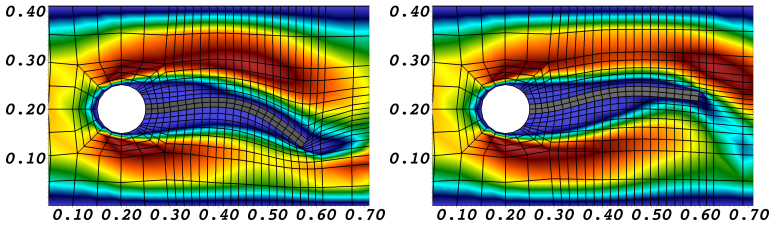

Fig. 3 Velocity field and mesh deformation at two snapshots using the harmonic MMPDE. The displacement extremum is displayed at left and a small deformation is shown at right. These two time instances also refer to Table 1, where the respective Newton iterations are measured.

The discretization parameters for time and space are chosen as follows. We choose $k = 0.2s, 0.1s, 0.05s, 0.01s, 0.005s, 0.0025s$. The first two (large) time step sizes are mainly to show that the formulation still works but that k is too large to capture the physics; namely that beam oscillations correctly develop. To have a fair comparison about the computational cost all examples are computed until $T = 15s$.

This corresponds to 150 solves using $k = 0.1s$ and 6000 solves using $k = 0.00025s$. The initial mesh without any refinements does not yield any oscillations. Thus, we refine once, twice and three-times uniformly leading to the mesh levels $1, 2, 3$ with

748 cells and 14740 $(6248+6248+2244)$ and 20988 $(6248+6248+2244+6248)$ DoFs
2992 cells and 57904 $(24464+24464+8976)$ and 82368 $(24464+24464+8976+24464)$ DoFs
11968 cells and 229504 $(96800+96800+35904)$ and 326304 $(96800+96800+35904+96800)$ DoFs

In the last two columns the degrees of freedom (DoFs) for the 2nd order models and the 4th order biharmonic model are shown, respectively.

Programming code and computing machines

As programming code, the serial open-source code published in [18] has been employed for the biharmonic MMPDE with four basic unknowns $\{\hat{v}, \hat{p}, \hat{u}, \hat{\eta}\}$. For the 2nd order models, this code has been modified for solving second order models with three basic unknowns $\{\hat{v}, \hat{p}, \hat{u}\}$. The examples were run on a Intel(R) Xeon(R) CPU W3680 with 3.33GHz desktop (machine 1). To highlight the dependence on hardware configurations, we also computed the biharmonic MMPDE on a Intel(R) Core(TM) i5-3320M CPU 2.60GHz laptop (machine 2).

Goals of our investigations

- Compare all three MMPDEs w.r.t. to quantities of interest;
- Compare all three MMPDEs w.r.t. to computational cost;
- Temporal and spatial convergence of the quantities of interest.

Discussion of the results

In our findings, we observe in Figure 4 that the u_y displacements are similar. The mesh regularity becomes better using a more sophisticated MMPDE as displayed in Figure 5. First, the nonlinear harmonic model is still able to compute this test with a minimal $\hat{J} = 0.045 - 0.02$ compared to a twice better $\hat{J} = 0.094 - 0.05$ (using the elastic MMPDE) and a 10 times better $\hat{J} = 0.445 - 0.40$ using biharmonic mesh motion (see Table 1 and 2). These differences are reflected in the number of Newton iterations which in the extremum points with largest solid deformations are two times higher for the second order models compared to the biharmonic MMPDE.

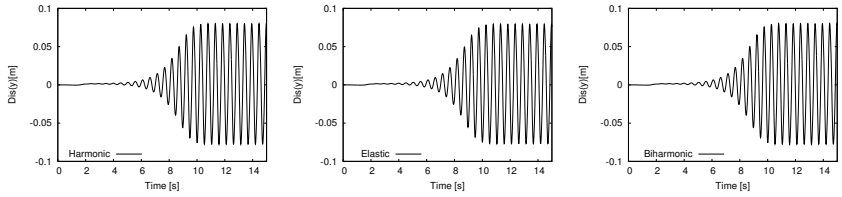

Fig. 4 Comparison of the u_y for nonlinear harmonic, nonlinear elastic and linear biharmonic mesh motion on mesh level 1 and $k = 0.01s$.

The number of Jacobian assemblies is approx. 3–4 times higher using second order models. The total computational cost differs slightly between the second order

models. Observing the Tables 1, 2, 3, our findings indicate that for this FSI benchmark, the biharmonic mesh motion model is competitive due to better regularity of the ALE mapping and less Newton iterations despite higher cost in each linear solve. The accuracy of goal functional evaluations with respect to the different MMPDEs, temporal and spatial refinement and different time-stepping schemes are shown in the Figures 6, 7, 8, and 9.

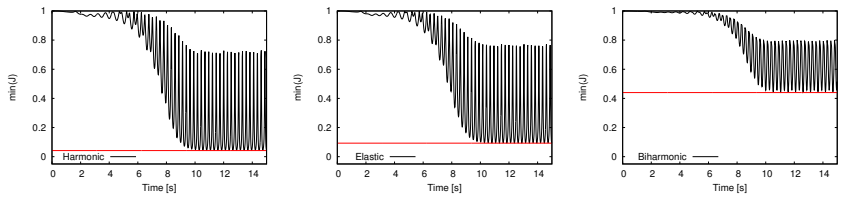

Fig. 5 Comparison of the mesh regularity for level 1 and $k = 0.01s$ in terms of $\min(\hat{J})$ for nonlinear harmonic, nonlinear elastic and linear biharmonic mesh motion.

Table 1 Comparison of Newton iterations for 1-times global refinement and $k = 0.01s$, the minimal $\hat{J}$, number of assembling the Jacobian, solving the linear system, and the total computational cost.

	Harmonic	Elastic	Biharmonic
Newton iter (extremum; Fig. 3 (left))	59	59	17
Newton iter (small deform.; Fig. 3 (right))	8	8	8
$\min(\hat{J})$	0.045	0.094	0.445
Assembling the Jacobian matrix (total no.)	20014	20701	6746
Solve linear system (total no.)	22108	22801	10747
Computational cost (total CPU time)	$4.737 \times 10^4 s$	$5.148 \times 10^4 s$	$6.638 \times 10^4 s$

Table 2 Comparison of Newton iterations for 2-times global refinement and $k = 0.0025s$, the minimal $\hat{J}$, number of assembling the Jacobian, solving the linear system, and the total computational cost.

	Harmonic	Elastic	Biharmonic
Newton iter (extremum; Fig. 3 (left))	59	59	15
Newton iter (small deform.; Fig. 3 (right))	8	8	6
$\min(\hat{J})$	0.02	0.05	0.40
Assembling the Jacobian matrix (total no.)	102809	96674	24173
Solve linear system (total no.)	110129	104135	36015
Computational cost (total CPU time)	$1.430 \times 10^6 s$	$1.398 \times 10^6 s$	$1.527 \times 10^6 s$

We emphasize that transient fluid-structure interaction for long-term simulations on fine meshes is infeasible using serial programming. Further comparisons of the harmonic and biharmonic MMPDEs on mesh level 3 and time step size $k = 0.01s$ yield that the former model runs almost 31 days and the biharmonic model runs 39 days on machine 1.

Table 3 Comparison of the costs for mesh level 1 and $k = 0.01s$ for two different machines.

	Machine 1	Machine 2
Harmonic: Cost per linear solve	$1.5s - 2.22s$	$0.6s - 1.65s$
Harmonic: Computational cost (total CPU time)	$4.737 \times 10^4 s$	$3.183 \times 10^4 s$
Elastic: Cost per linear solve	$1.55s - 2.4s$	$0.64s - 1.7s$
Elastic: Computational cost (total CPU time)	$5.148 \times 10^4 s$	$3.304 \times 10^4 s$
Biharmonic: Cost per linear solve	$5.65s - 6.7s$	$1.57s - 3.02s$
Biharmonic: Computational cost (total CPU time)	$6.638 \times 10^4 s$	$2.609 \times 10^4 s$

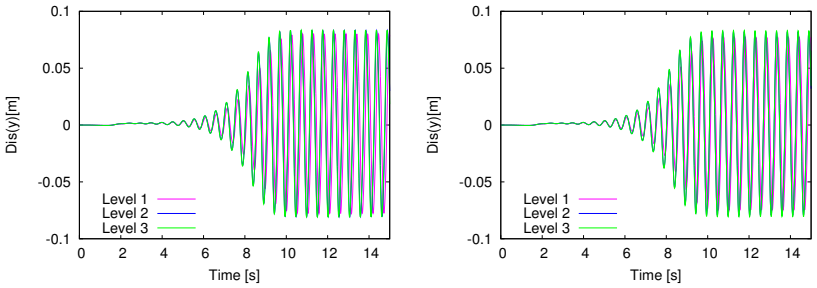

Fig. 6 Comparison of u_y for a fixed time step size $k = 0.01s$ and three different mesh levels. On the left the nonlinear harmonic MMPDE is shown and on the right the biharmonic model.

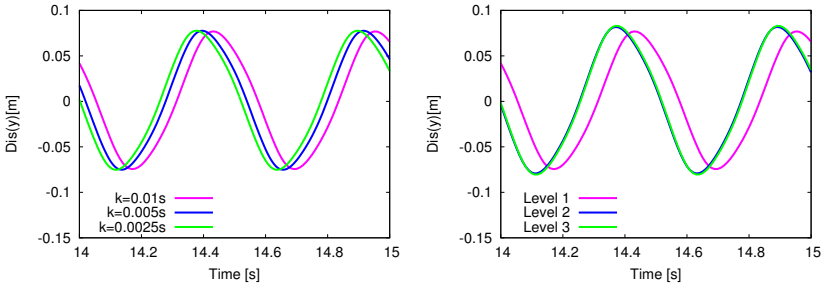

Fig. 7 Comparison of u_y using the biharmonic MMPDE. On the left a zoom-in for temporal convergence (on Level 1) is shown and on the right spatial convergence for $k = 0.01s$ is plotted.

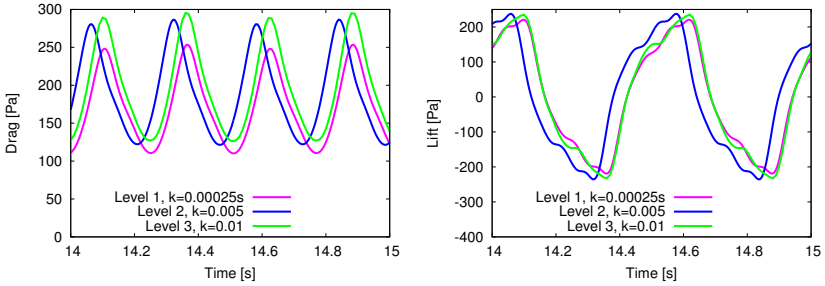

Fig. 8 Comparison of drag (left) and lift (right) using the biharmonic MMPDE. Here, we make a rather unusual comparison: refining the mesh level while coarsening the time step size. For the drag and the lift we observed less accurate results (not shown here) for the harmonic and elastic MMPDE - in particular when the beam has its largest deformations.

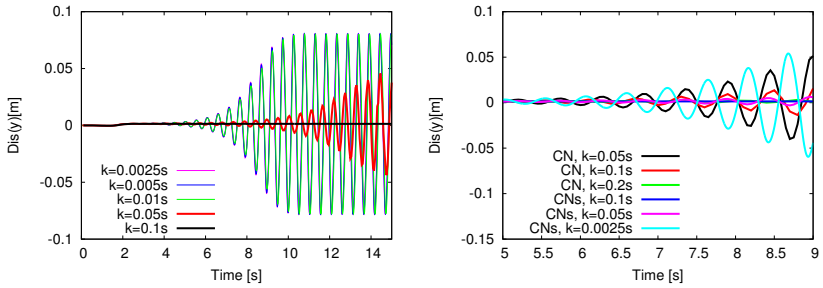

Fig. 9 Comparison of u_y on mesh level 1 and different time step sizes k using the shifted Crank-Nicolson (CNs) scheme (left) and a comparison with the classical Crank-Nicolson (CN) method (right). First thanks to the monolithic formulation and implicit time-stepping we are able to use large time steps, e.g., $k = 0.2s$. Secondly, the large time step is not sufficient any more to lead to the correct oscillations of the elastic beam. In particular, care of the correct choice of the damping factor using the shifted version must be taken. From this figure, we infer that the largest time step size is around $k \sim 0.01s$ in order to obtain the correct amplitude of oscillations.

5 Conclusions

In this study we found that biharmonic mesh motion for ALE-FSI has competitive computational cost for long-term simulations with many time steps. Using biharmonic mesh motion, the higher fluid-mesh regularity for large solid deformations does lead to much less Newton iterations per time step and consequently the higher cost in the linear solver is (almost) compensated. On the other hand, for moderate deformations, it is still absolutely sufficient to use a (linear) second order mesh motion model rather than a 4th order equation. Moreover, this variational-monolithic formulation works for implicit A-stable time-stepping schemes with large time steps. However, if the time step is chosen too large the physics of the problem are not correctly represented. Finally, all three mesh motion models converge under temporal and spatial refinement while goal functionals show the same quantitative behavior.

References

1. Bazilevs, Y., Takizawa, K., Tezduyar, T.: Computational Fluid-Structure Interaction: Methods and Applications. Wiley (2013)
2. Budd, C.J., Huang, W., Russell, R.D.: Adaptivity with moving grids. Acta Numerica **18**, 111–241 (2009). DOI 10.1017/S0962492906400015
3. Bungartz, H.J., Schäfer, M.: Fluid-Structure Interaction: Modelling, Simulation, Optimization, *Lecture Notes in Computational Science and Engineering*, vol. 53. Springer (2006)
4. Donea, J., Giuliani, S., Halleux, J.: An arbitrary lagrangian-eulerian finite element method for transient dynamic fluid-structure interactions. Comput. Methods Appl. Mech. Engrg. **33**, 689–723 (1982)

5. Dunne, T., Richter, T., Rannacher, R.: Numerical simulation of fluid-structure interaction based on monolithic variational formulations, pp. 1–75. Comtemporary Challenges in Mathematical Fluid Mechanics. Springer, World Scientific, Singapore (2010)
6. Formaggia, L., Nobile, F.: A stability analysis for the arbitrary Lagrangian Eulerian formulation with finite elements. East-West Journal of Numerical Mathematics **7**, 105 – 132 (1999)
7. Helenbrook, B.: Mesh deformation using the biharmonic operator. Int. J. Numer. Methods Engrg. pp. 1–30 (2001)
8. Heywood, J.G., Rannacher, R.: Finite-element approximation of the nonstationary Navier-Stokes problem part iv: Error analysis for second-order time discretization. SIAM Journal on Numerical Analysis **27**(2), 353–384 (1990)
9. Heywood, J.G., Rannacher, R., Turek, S.: Artificial boundaries and flux and pressure conditions for the incompressible Navier-Stokes equations. International Journal of Numerical Methods in Fluids **22**, 325–352 (1996)
10. Hron, J., Turek, S.: Proposal for numerical benchmarking of fluid-structure interaction between an elastic object and laminar incompressible flow, vol. 53, pp. 146 – 170. Springer-Verlag (2006)
11. Hughes, T., Liu, W., Zimmermann, T.: Lagrangian-Eulerian finite element formulation for incompressible viscous flows. Comput. Methods Appl. Mech. Engrg. **29**, 329–349 (1981)
12. Rannacher, R.: On the stabilization of the Crank-Nicolson scheme for long time calculations (1986). Preprint
13. Richter, T., Wick, T.: On time discretizations of fluid-structure interactions. In: T. Carraro, M. Geiger, S. Körkel, R. Rannacher (eds.) Multiple Shooting and Time Domain Decomposition Methods, pp. 377–400. Contributions in Mathematical and Computational Science (2015). URL http://www.springer.com/us/book/9783319233208
14. Stein, K., Tezduyar, T., Benney, R.: Mesh moving techniques for fluid-structure interactions with large displacements. J. Appl. Mech. **70**, 58–63 (2003)
15. Tezduyar, T.E., Behr, M., Mittal, S., Johnson, A.A.: Computation of Unsteady Incompressible Flows With the Finite Element Methods Space-Time Formulations, Iterative Strategies and Massively Parallel Implementations, *New Methods in Transient Analysis, PVP-Vol. 246, AMD-Vol. 143*, vol. 143, pp. 7–24. ASME, New York (1992)
16. Wick, T.: Adaptive Finite Element Simulation of Fluid-Structure Interaction with Application to Heart-Valve Dynamics. Ph.D. thesis, University of Heidelberg (2011). URL http://www.ub.uni-heidelberg.de/archiv/12992
17. Wick, T.: Fluid-structure interactions using different mesh motion techniques. Computers and Structures **89**(13-14), 1456–1467 (2011)
18. Wick, T.: Solving monolithic fluid-structure interaction problems in arbitrary Lagrangian Eulerian coordinates with the deal.II library. Archive of Numerical Software **1**, 1–19 (2013). URL http://www.archnumsoft.org
19. Wick, T.: Modeling, discretization, optimization, and simulation of fluid-structure interaction. Lecture notes at Heidelberg University and TU Munich (2015). URL https://www-m17.ma.tum.de/Lehrstuhl/LehreSoSe15NMFSIEn
20. Wick, T., Wollner, W.: On the differentiability of fluid-structure interaction problems with respect to the problem data. RICAM report 2014-16 available on http://www.ricam.oeaw.ac.at/publications/reports/ (2014)
21. Winslow, A.M.: Numerical solution of the quasilinear poisson equation in a nonuniform triangle mesh. Journal of Computational Physics **1**(2), 149 – 172 (1966)
22. Yigit, S., M. Schäfer, M.H.: Grid movement techniques and their influence on laminar fluid-structure interaction problems. J. Fluids and Struct. **24**(6), 819–832 (2008)